

Structural and transport properties of α-$RbCu_4Cl_3I_2$ at room temperature by molecular dynamics simulation

Yueqiang Lan(兰越强), Tushagu Abudouwufu(吐沙姑·阿不都吾甫), Alexander Tolstoguzov, Dejun Fu(付德君)
Citation: Chin. Phys. B, 2025, 34 (**7**): 076501. DOI: 10.1088/1674-1056/adc18d
http://cpb.iphy.ac.cn; http://iopscience.iop.org/cpb

What follows is a list of articles you may be interested in

Thermal conductivity of iron under the Earth's inner core pressure

Cui-E Hu(胡翠娥), Mu-Xin Jiao(焦亩鑫), Xue-Nan Yang(杨学楠), Zhao-Yi Zeng(曾召益), and Jun Chen(陈军)
Chin. Phys. B, 2024, 33 (**10**): 106501. DOI: 10.1088/1674-1056/ad6078

Theoretical insights into thermal transport and structural stability mechanisms of triaxial compressed methane hydrate

Dong-Sheng Chen(陈东升), Ting-Ting Miao(缪婷婷), Cheng Chang(常程), Xu-Yang Guo(郭旭洋), Meng-Yan Guan(关梦言), and Zhong-Li Ji(姬忠礼)
Chin. Phys. B, 2024, 33 (**9**): 096501. DOI: 10.1088/1674-1056/ad57ae

Phonon transport properties of Janus Pb_2XAs(X = P, Sb, and Bi) monolayers: A DFT study

Jiaxin Geng(耿嘉鑫), Pei Zhang(张培), Zhunyun Tang(汤准韵), and Tao Ouyang(欧阳滔)
Chin. Phys. B, 2024, 33 (**4**): 046501. DOI: 10.1088/1674-1056/ad2260

Transport properties of CrP

Xuebo Zhou(周学博), Ping Zheng(郑萍), Wei Wu(吴伟), Yu Sui(隋郁), and Jianlin Luo(雒建林)
Chin. Phys. B, 2023, 32 (**7**): 076501. DOI: 10.1088/1674-1056/acc80c

Structural phase transition and transport properties in topological material candidate $NaZn_4As_3$

Qing-Xin Dong(董庆新), Bin-Bin Ruan(阮彬彬), Yi-Fei Huang(黄奕飞), Yi-Yan Wang(王义炎), Li-Bo Zhang(张黎博), Jian-Li Bai(白建利), Qiao-Yu Liu(刘乔宇), Jing-Wen Cheng(程靖雯), Zhi-An Ren(任治安), and Gen-Fu Chen(陈根富)
Chin. Phys. B, 2023, 32 (**6**): 066501. DOI: 10.1088/1674-1056/acbe2f

---

Structural and transport properties of α-$RbCu_4Cl_3I_2$ at room temperature by molecular dynamics simulation

Yueqiang Lan(兰越强)[1,2], Tushagu Abudouwufu(吐沙姑·阿不都吾甫)[1,2], Alexander Tolstoguzov[2,3,4], and Dejun Fu(付德君)[1,2,†]

[1] *Key Laboratory of Artificial Micro and Nanostructures of the Ministry of Education and Hubei Key Laboratory of Nuclear Solid Physics, School of Physics and Technology, Wuhan University, Wuhan* 430072, *China*

[2] *Zhuhai Tsinghua University Research Institute Innovation Center, Zhuhai* 519000, *China*

[3] *Utkin Ryazan State Radio Engineering University, Gagarin Str.* 59/1, 390005 *Ryazan, Russian Federation*

[4] *Centre for Physics and Technological Research, Universidade Nova de Lisboa, Caparica* 2829-516, *Portugal*

(Received 12 November 2024; revised manuscript received 28 February 2025; accepted manuscript online 18 March 2025)

Considering α-$RbCu_4Cl_3I_2$ is isostructural with α-$RbAg_4I_5$, in this work, we built a molecular dynamics simulation system of the former superionic conductor with an empirical pairwise potential model, which was verified on the latter crystal, including long-ranging Coulomb, short-ranging Born–Mayer, charge–dipole, and dipole–quadrupole interactions. The corresponding parameters were collected from the crystal structure and several reports of interionic potentials in alkali halides. The coordination number of fixed ions was examined, and the dynamic distribution of dissociative Cu^+ was described by the radial distribution function. The diffusion behavior of the ions was evaluated with mean square displacements and velocity auto-correlation functions. The diffusion coefficient of copper ions obtained is $(47.9\pm6.1)\times10^{-7}$ cm^2/s, which is approximately 37 times that of the simulation result $(1.3\pm0.1)\times10^{-7}$ cm^2/s of silver in α-$RbAg_4I_5$ at room temperature. In this work, the diffusion coefficient of Cu^+ was first discussed by molecule simulation, while there are few experimental reports.

Keywords: diffusion coefficients, Cu^+ conductors, superionic conductor, microcanonical ensemble, empirical pair potential

PACS: 65.40.–b, 66.30.H–, 66.10.Ed, 82.20.Wt

DOI: 10.1088/1674-1056/adc18d **CSTR:** 32038.14.CPB.adc18d

1. Introduction

Nowadays, the discovery and development of solid electrolytes benefit human beings in the energy storage of mobile devices. The massive demand for lighter, safer, longer-lasting energy storage and lower-cost batteries is attracting researchers and arousing many investigations and applications on Li^+ and Na^+ ion electrolytes.[1–3] Additionally, machine learning methods are applied to predict Li^+, Zn^+, and Al^+ battery cathode materials satisfying the criteria from massive materials with fast screening.[4] In contrast, the recognition and study of Cu^+,[5–9] Ag^+,[10–21] and other mobile ions are much slower for the lack of these advantages of Li^+ and Na^+ ions. However, it is worth pushing forward that the potential usages on micro-thruster of satellites, field emission ion implantation of the Cu^+ or Ag^+ achieving interconnection on three-dimensional (3D) integrated circuit (IC) chips,[22] designing memristor by Ag alloyed with Cu in an Si medium,[23] and so on.

The compound α-$RbAg_4I_5$ was discovered in 1967 (see Refs. [24,25]) with excellent room temperature conductivity of 0.27 S/cm.[26] Later on, the crystal structure of α-$RbCu_4Cl_3I_2$ with further ion conductivity of 0.47 S/cm was reported by Geller[8] in 1979, after α-$Rb_4Cu_{16}Cl_{13}I_7$ with 0.34 S/cm by Takahashi in the same year.[9] They are both isostructural with α-$RbAg_4I_5$. In α-$RbCu_4Cl_3I_2$, all the tetrahedra have Cl^- and I^- ions at apices, but the coordination polyhedron about the Rb^+ ions contain only Cl^- ions. The transition of α–β and β–γ phases occurs at 221 K and 170 K, respectively.

The exploration of the theoretical model description on atomic level for alkali halides[27–31] and superionic conductors[11,13,19,21,32–38] subsequently emerged following the experimental result.[26,28,39–41] In 2019, by molecular dynamic (MD) simulation, Burbano *et al.* constructed the dynamic model of α-$RbAg_4I_5$ with an empirical pairwise potential of four terms and calculated the diffusion coefficient $D_{MD} = (0.13\pm0.1)\times10^{-6}$ cm^2/s comparing with the experimental results $D_{NMR} = (0.18\pm0.1)\times10^{-6}$ cm^2/s at room temperature.[19] The following year, the diffusion path of Ag^+ ions[11] was studied using the same simulation model, and some new sites were reported.[13] These numerical simulations make a significant theoretical contribution to understanding the mechanism of the behavior of solid electrolytes on an atomic scope.

Meanwhile, a battery prototype, the solid electrolyte cell, copper–$RbCu_4Cl_3I_2$–I_2, glassy carbon studied by Ostapenko in 2000,[42] and the iodine diffusion coefficient limiting the

†Corresponding author. E-mail: djfu@whu.edu.cn

© 2025 Chinese Physical Society and IOP Publishing Ltd. All rights, including for text and data mining, AI training, and similar technologies, are reserved.

chemical interaction of iodine with $RbCu_4Cl_3I_2$ was 6.2×10^{-7} cm^2/s. In 2001, the author also studied the cell of Cu/$RbCu_4Cl_3I_2$/Pt, and the diffusion coefficient of Cu^{2+} between a 1-μm-thick layer of Cu_2O and $RbCu_4Cl_3I_2$ interface is 0.15×10^{-7} cm^2/s,[43] limiting the reaction rate of $Cu^+ - e^- \rightleftharpoons Cu^{2+}$. These two pieces of research suggested that the diffusion coefficient of Cu^+ in $RbCu_4Cl_3I_2$ is tremendously beyond the above limitations.

Given that there is little research about α-$RbCu_4Cl_3I_2$ with the MD modeling. This work aims to build the MD simulation system of $RbCu_4Cl_3I_2$ at room temperature using the method in the work of Burbano *et al.*[19] The crystal model refers to the structure data on the experimental result,[8] and some potential parameters are collected from the research of alkali halides.[27–29]

2. Methods

MD simulation on the MolDy program is applied with classical Newton's equation. The empirical potential is used to describe the structural and dynamical properties in $RbCu_4Cl_3I_2$ at room temperature:

$$U_{ij}(r) = \frac{Z_i Z_j e^2}{4\pi\varepsilon_0}\frac{1}{r} + bc_{ij}\exp\left[\frac{\sigma_i+\sigma_j-r}{\rho}\right] - \frac{P_{ij}}{r^4} - \frac{W_{ij}}{r^6}. \tag{1}$$

The first term is the Coulomb interaction with long range. The second term is overlap repulsive interaction (Born–Mayer potential) with short range assuming that ions are rigid spheres. The third and fourth terms are mono-dipole-induced and dipole–dipole interactions considering each ions having a polarized attribute. Z_i and Z_j are the effective charge of the corresponding ions. The parameter b is 20.8 kJ/mol[32] ρ is a constant value of 1/3 Å, and c_{ij} is expressed as

$$c_{ij} = 1 + \frac{Z_i}{N_i} + \frac{Z_j}{N_j}, \tag{2}$$

where N_i or N_j denotes the number of electrons in the outer shells of the corresponding ion.[44] For example, the Rb^+ is 8, Cu^+ is 18, Cl^- is 8, and I^- is 8.P_{ij} has the following equation:

$$P_{ij} = \frac{\left(\alpha_i Z_j^2 + \alpha_j Z_i^2\right)e^2}{8\pi\varepsilon_0}, \tag{3}$$

where α_i or α_j is the polarizability of the corresponding ion.

In Table 1, the effective radius of the ions are collected from the work of Gellar[8] in 1979 in which the radius of I^- ions is determined by the minimized length of the I–I bond, the same of Cl^-, then based on the minimized length of Rb–I bond the Rb radius is identified. At last, the minimized length of the Cu–I or Cu–Cl pair determines the radius of Cu^+. The polarizability of each ion at 300 K is from the work of Jaswal and Sharma in 1972,[39] except that ions of copper are zero since they almost wander in the gap of the crystal.

Table 1. Values for the ionic parameter as the effective radii (σ), polarizability (α), and effective charge (Z).

Ion	σ (Å)	α (Å^3)	Z
Rb^+	1.521	1.707	0.63
Cu^+	0.45	0	0.63
Cl^-	1.87	3.004	–0.63
I^-	2.114	6.294	–0.63

The coefficient W_{ij} of each pair of ions can be found in the review of Sangster *et al.* in 1976,[28] except Cl–I. However, given the equation

$$W_{ij} = \frac{3}{2}\frac{\alpha_i\alpha_j E_i E_j}{E_i + E_j}, \tag{4}$$

the W_{ij} can also be derived as

$$W_{ij} = 2\frac{\alpha_i^2\alpha_j^2 W_{ii}W_{jj}}{\alpha_i^2 W_{jj} + \alpha_j^2 W_{ii}}, \tag{5}$$

thus, W_{ij} of the pairs of Cl–I can be estimated from the values of Cl–Cl and I–I.

3. Results

After the Coulomb interaction term, the MolDy program provides additional potential models, such as Lennard–Jones, 6-exp, MCY, and generic potentials. Only the last one fitting the formation of Eq. (1) is expressed as

$$U = p_0 e^{-p_1 r} + \frac{p_2}{r^{12}} - \frac{p_3}{r^4} - \frac{p_4}{r^6} - \frac{p_5}{r^8}, \tag{6}$$

where the parameters of α-$RbCu_4Cl_3I_2$ are listed in Table 2. p_0 and p_1 contribute to the strength of repulsion referenced from Fumi and Tosi repulsive parameters. The former is determined by the radius of the two particles and the latter varies slightly around 3 for different rocksalt structure alkali halides including RbCl, and RbI.[28] p_3 is corresponding to the parameter of P_{ij} and p_4 is W_{ij} which is derived from Table 4 of Ref. [28].

α-$RbCu_4Cl_3I_2$ is calculated with the $P4_132$ space group at 300 K in the NVE ensemble. The Ewald method is applied to calculate the Coulomb interaction. A unit cell of α-$RbCu_4Cl_3I_2$ with 26 neighbor cells contains 27×40 ions ($Rb^+ = 432$, $Cu^+ = 108$, $Cl^- = 324$, and $I^- = 216$). Then, the periodic boundary condition is applied to extend to endless numbers of the same prototype in three directions to approximate the macroscope condition and avoid the surface transition calculation. The MD step is set up to be one fs. The heating up of the system with the extra kinetic energy transferred from the extra repulsive potential of the lag reaction of finite element calculation when the collision of ions occurs is inevitable, especially in a significant slope potential. Thus, temperature rescaling is necessary throughout the whole simulation. The MD run is separated into two phases. The first phase is set up with 5×10^6 steps (5000 ps) to equilibrium the system. The second phase contains 10×10^6 steps (10^4 ps), and the data of the last 5000 ps are taken to make analyses.

Table 2. Values of the parameters for each ion pair in α-$RbCu_4Cl_3I_2$ at room temperature.

Ion pair	p (kJ/mol)	p_1 (Å^{-1})	p_2 (kJ·Å^{12}/mol)	p_3 (kJ·Å^4/mol)	p_4 (kJ·Å^6/mol)	p_5 (kJ·Å^8/mol)
Rb–Rb	2.213×10^5	3	0	9.413×10^2	3.577×10^3	0
Rb–Cu	8.567×10^3	3	0	4.706×10^2	0	0
Rb–Cl	5.447×10^5	3	0	1.299×10^3	4.757×10^3	0
Rb–I	1.133×10^6	3	0	2.206×10^3	8.130×10^3	0
Cu–Cu	3.312×10^2	3	0	0	0	0
Cu–Cl	2.096×10^4	3	0	8.283×10^2	0	0
Cu–I	4.357×10^4	3	0	1.735×10^3	0	0
Cl–Cl	1.307×10^6	3	0	1.657×10^3	7.829×10^3	0
Cl–I	2.718×10^6	3	0	2.564×10^3	1.406×10^4	0
I–I	5.652×10^6	3	0	3.471×10^3	2.577×10^4	0

The evolution of the temperature and the total energy in the second phase showing in Fig. 1 verify the equilibration of the system. The average temperature and the total energy per primitive cell of α-$RbCu_4Cl_3I_2$ are 300.1±2.1 K and -104.56 ± 0.04 eV, respectively. Here, the total energy of α-$RbAg_4I_5$ is -95.798 ± 0.012 eV per unit cell rather than 23.9495±0.003 eV per mole expressed in Burbano's work. The corresponding temperature of the component average velocity $T_x = 295.6$ K, $T_y = 304.6$ K, and $T_z = 297.4$ K of Cu^+ agree well with the Maxwell distribution.

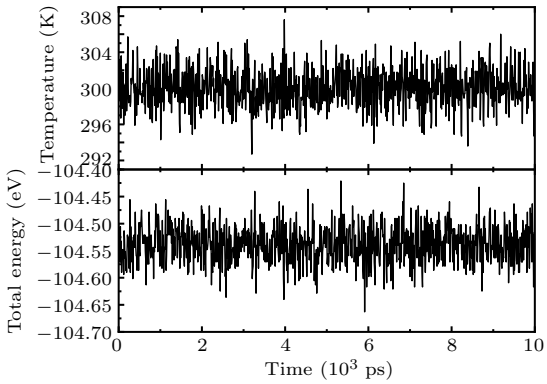


Fig. 1. The evolution of the temperature and the total energy for $RbCu_4Cl_3I_2$ along the second phase.

Radial distribution function (RDF) $g(r)$ is used to show the structure of crystal materials. The coordination number can be revealed when the integration of $g(r)$ in spherical coordinates is multiplied by the number of the right-side partner particles in the unit cell. A normalized $g(r)$ profile always tends to be 1 in the bulk range. The $g(r)$ of Rb–Rb, Cu–Cu, Cl–Cl, and I–I pair are shown in Fig. 2(a), while the coordination number of Rb surrounding itself is six at 6.15 Å, Cl is four at 3.65 Å, and I is three at 4.175 Å while one more at 4.8 Å as shown in Fig. 2(c). The $g(r)$ of Rb–Cl surrounding Rb is six at 3.4 Å, I surrounding Rb is six at 4.25 Å, and I surrounding Cl is six at 4.075 Å as shown in Figs. 2(b) and 2(d). The image demonstrations are shown in Fig. 3. These coordination numbers demonstrated agree well with the structure of α-$RbCu_4Cl_3I_2$ (Ref. [8]) in the tolerance of accuracy range of ±0.025 Å.

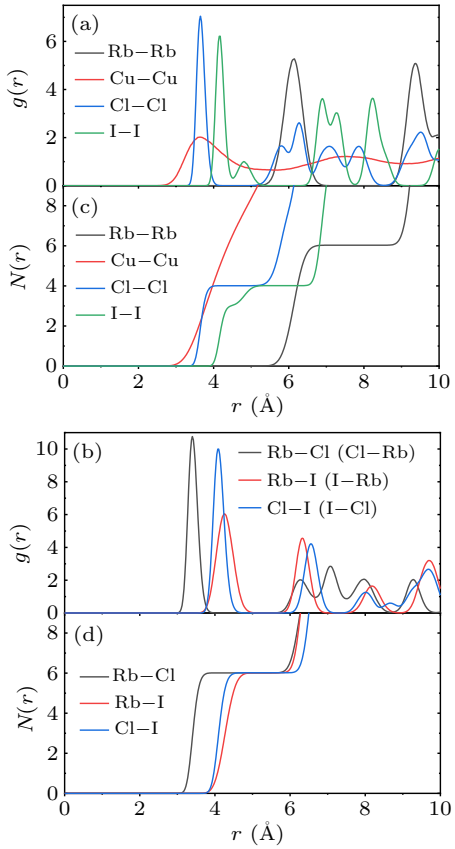


Fig. 2. RDF for the pairs of (a) Rb–Rb, Cu–Cu, Cl–Cl, I–I; (b) Rb–Cl (Cl–Rb), Rb–I (I–Rb), Cl–I (I–Cl); and the coordination numbers (first platform) of (c) Rb–Rb, Cu–Cu, Cl–Cl, I–I; (d) Rb–Cl, Rb–I, Cl–I in the crystal α-$RbCu_4Cl_3I_2$ at room temperature.

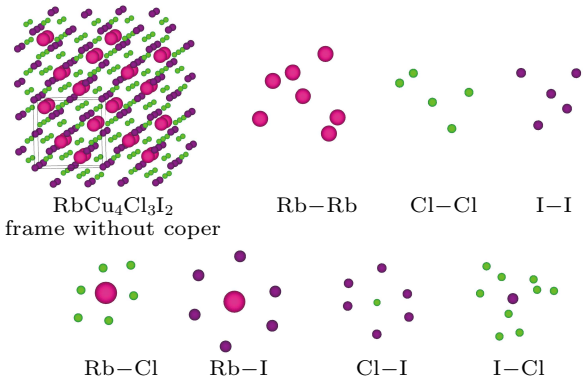


Fig. 3. Image demonstration of coordination numbers of fixed ion pair of α-$RbCu_4Cl_3I_2$, the balls with red, green, and purple curlers representing Rb^+, Cl^-, and I^-, respectively.

The $g(r)$ of Cu–Cu in Fig. 3(a) with a smoother curve indicates that Cu^+ is almost free in the crystal. The first three peaks of Cu^+ distribute at 3.65 Å, 7.55, Å, and 10.225 Å, while Ag^+ is 4.45 Å, 8 Å, and 11.2 Å, which of these are shown in Fig. 4. The first peak of Cu^+ surrounding Rb^+, Cl^-, and I^- is 3.825 Å, 2 Å, and 2.45 Å, respectively, while Ag^+ surrounding Rb^+ and I is 4.225 Å and 2.7 Å, respectively.

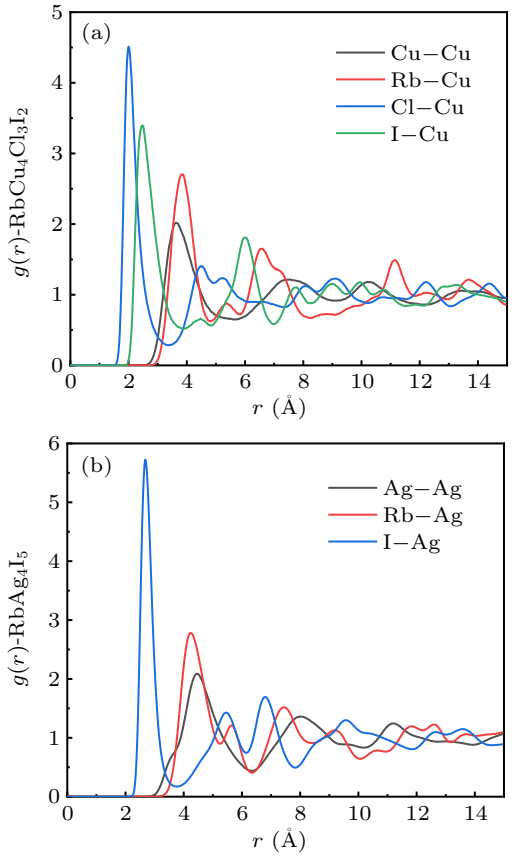


Fig. 4. Comparisons of RDF between free ions, (a) Cu^+ and (b) Ag^+ surround itself and fixed ions in $RbCu_4Cl_3I_2$ and $RbAg_4I_5$, respectively, at room temperature.

The profiles of mean square displacements (MSDs) and velocity auto-correlation functions (VAFs) of each particle typically reveal the dynamic properties of the equilibrium system. The line of MSD for each particle of the crystals is compared in Fig. 5. The relatively stable MSD value of Rb^+ is 1.027 $Å^2$, Cl^- is 0.947 $Å^2$, I^- is 0.936 $Å^2$ in $RbCu_4Cl_3I_2$ after a long enough simulation time, indicating that they are almost vibrating at the fixed area. Meanwhile, the line of Cu^+ is 100.45 $Å^2$ at 300 ps and 861.86 $Å^2$ at 3000 ps. Here, it should be corrected that the mistake of the MSD profile in the work of Burbano *et al.*,[19] where the time steps range is 3000 ps instead of 300 ps. The corresponding estimated diffusion coefficient is shown in Table 3. The slope at 300 ps and 3000 ps reveals the corresponding coefficient values. Because of the cage effects the value of former is large than the latter. $D_{(\infty)}$ is evaluated from the average slope along 3000 ps. The value of error ±6.1 is the deviation of slope along 3000 ps.

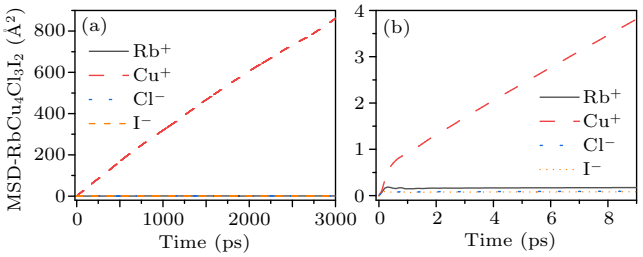


Fig. 5. MSD calculated by MD simulation at room temperature for each ion of α-$RbCu_4Cl_3I_2$ in the range of 3000 ps (a) and (b) 9 ps.

Table 3. Calculated diffusion coefficient with varied scale simulation time.

	$D_{(300\ \mathrm{ps})}$ (10^{-7} cm^2/s)	$D_{(3000\ \mathrm{ps})}$ (10^{-7} cm^2/s)	$D_{(\infty)}$ (10^{-7} cm^2/s)
Cu^+ in α-$RbCu_4Cl_3I_2$	55.8	47.9	47.9±6.1

The VAFs are calculated to examine the dynamical properties. The algorithm of normalized VAFs is

$$\mathrm{VAFs}(t) = \frac{\langle v_i(t_0)\cdot v_i(t_0+t)\rangle}{\langle v_i(t_0)\cdot v_i(t_0)\rangle}, \tag{7}$$

where v_i denotes the velocity of particles, t_0 denotes the start time for counting, and t is the evolution time of VAFs. The curves of each ion in the material are illustrated in Fig. 6. The fixed ions, Rb^+, Cl^-, and I^-, have an oscillatory profile, while Cu^+ shows a fast, decent correlation profile, and agrees with the feature of wandering in the crystal.

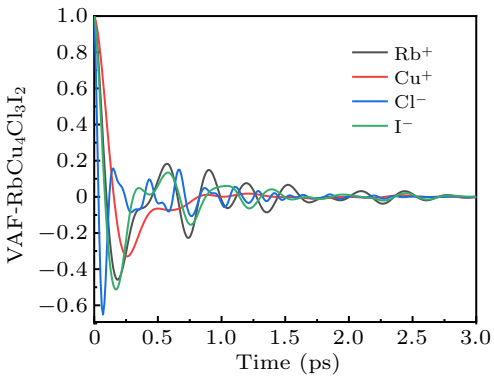


Fig. 6. VAF for each ion of α-$RbCu_4Cl_3I_2$ in the time range of 3 ps.

The diffusion coefficient of Cu^+ also can be calculated from the equation

$$D_{\mathrm{VAF}} = \frac{1}{3}\int_{t=0}^{t=t_{\max}} \langle v_i(t_0)\cdot v_i(t_0+t)\rangle\,\mathrm{d}t. \tag{8}$$

The calculated value $D_{\mathrm{VAF}} = 31.716\times10^{-7}$ cm^2/s is smaller than that from MSD. However, the sample is not large enough, and this value will not be considered.

4. Conclusion

In summary, we used a proper method and the experiment parameters to build the MD simulation system for α-$RbCu_4Cl_3I_2$ at room temperature and obtain the structural and

transport properties. The RDF profiles of each fixed ion kept the original structure during the simulation and the RDF of Cu^+ shows the dynamic distribution in the crystal gap. MSD profiles were calculated to estimate the diffusion coefficient, which for Cu^+ in $RbCu_4Cl_3I_2$ was $(47.9 \pm 0.61) \times 10^7$ cm^2/s and approximately 37 times that of the simulation result $(1.3 \pm 0.1) \times 10^{-7}$ cm^2/s of Ag^+ in α-$RbAg_4I_5$. In the work of Ostapenko *et al.* about the solid electrolyte cell,[41] copper-$RbCu_4Cl_3I_2$–I_2, the diffusion coefficient value iodine diffusion 6.2 $\times 10^{-7}$ cm^2/s depending on porosity and on the history of the $RbCu_4Cl_3I_2$ sample limiting the decomposition of electrolyte maybe provide the only clue for the discrepancy of Cu^+ and Ag^+. However, too small value of Cu^+ or the other fixed ions radius determined by the method in our work that maybe make the discrepancy big, thus the slight tuning of each radius to fit the experimental dates remaining to study in the future. The VAFs profile also shows the free feature of Cu^+. This work first reported the diffusion coefficient of Cu^+ in α-$RbCu_4Cl_3I_2$ at room temperature and paved the way for understanding the structural and transport properties of Cu^+ in solid electrolytes.

Acknowledgements

Project supported by the National Natural Science Foundation of China (Grant Nos. 12375285 and U2430205) and the China Postdoctoral Science Foundation (Grant No. 2022M722439). We thank Dr. Pavel Stishenko from Cardiff University for providing valuable advice in this work.

References

[1] Bedrov D, Borodin O and Hooper J B 2017 *J. Phys. Chem. C* **121** 16098
[2] Li M, Lu J, Chen Z and Amine K 2018 *Adv. Mater.* **30** 1800561
[3] Whittingham M S 2020 *Nano Lett.* **20** 8435
[4] Liu X, Yang K, Zhang L, Wang W, Zhou S, Wu B, Xiong M, Yang S and Tan R 2024 *Energy Mater. Adv.* **5** 0131
[5] Abudouwufu T, Zhang X, Zuo W, Pelenovich V, Luo J, Lan Y, Tian C, Zou C, Tolstoguzov A and Fu D 2022 *Vacuum* **196** 110742
[6] Reznitskikh O G, Yaroslavtseva T V, Glukhov A A, Popov N A, Urusova N V, Bukun N G, Dobrovolsky Yu A and Bushkova O V 2022 *Russ. J. Electrochem.* **58** 927
[7] Takahashi T, Kuwabara K, Miura M and Nakanishi M 1982 *J. Appl. Electrochem.* **12** 213
[8] Geller S, Akridge J R and Wilber S A 1979 *Phys. Rev. B* **19** 5396
[9] Takahashi T, Yamamoto O, Yamada S and Hayashi S 1979 *J. Electrochem. Soc.* **126** 10
[10] Abudouwufu T, Zuo W, Pelenovich V, Zhang X, Zeng X, Tolstoguzov A, Zou C, Tian C and Fu D 2021 *Solid State Ionics* **364** 115634
[11] Burbano J C, Peña Lara D and Correa H 2020 *Phys. Status. Solidi. (b)* **257** 1900730
[12] Acharyya P, Ghosh T, Matteppanavar S, Biswas R K, Yanda P, Varanasi S R, Sanyal D, Sundaresan A, Pati S K and Biswas K 2020 *J. Phys. Chem. C* **124** 9802
[13] Burbano J C, Correa H and Peña Lara D 2020 *Molecular Simulation* **46** 375
[14] Vivas E I, Peña Lara D and Alvaro G M 2021 *Ionics* **27** 781
[15] Zuo W B, Pelenovich V O, Tolstogouzov A B and Fu D J 2019 *IOP Conf. Ser.: Mater. Sci. Eng.* **668** 012021
[16] Zuo W, Pelenovich V O, Tolstogouzov A B, Ieshkin A E, Zeng X, Wang Z, Gololobov G, Suvorov D, Liu C, Fu D and Hu D 2019 *Vacuum* **167** 382
[17] Chen J L, Zuo W B, Ke X W, B Tolstoguzov A, Tian C X, Devi N, Jha R, N Panin G and Fu D J 2019 *Chin. Phys. B* **28** 060705
[18] Zuo W, Pelenovich V, Tolstogouzov A, Zeng X, Wang Z, Song X, Gusev S I, Tian C and Fu D 2019 *J. Alloys Compd.* **790** 109
[19] Burbano J C, Diosa J E and Peña Lara D 2019 *Molecular Simulation* **45** 724
[20] Daiko Y, Segawa K, Honda S and Iwamoto Y 2018 *Solid State Ionics* **322** 5
[21] Matsunaga S 2013 *Molecular Simulation* **39** 119
[22] Panigrahy A K and Chen K N 2018 *Journal of Electronic Packaging* **140** 010801
[23] Yeon H, Lin P, Choi C, Tan S H, Park Y, Lee D, Lee J, Xu F, Gao B, Wu H, Qian H, Nie Y, Kim S and Kim J 2020 *Nat. Nanotechnol.* **15** 574
[24] Bradley J N and Greene P D 1967 *Trans. Faraday Soc.* **63** 424
[25] Owens B B and Argue G R 1967 *Science* **157** 308
[26] Raleigh D O 1970 *J. Appl. Phys.* **41** 1876
[27] Ciccotti G, Jacucci G and McDonald I R 1976 *Phys. Rev. A* **13** 426
[28] Sangster M J L and Dixon M 1976 *Adv. Phys.* **25** 247
[29] Catlow C R A, Diller K M and Norgett M J 1977 *J. Phys. C: Solid State Phys.* **10** 1395
[30] Rice M J and Roth W L 1972 *J. Solid State Chem.* **4** 294
[31] Matsunaga S and Tamaki S 2011 *EPJ Web of Conferences* **15** 1
[32] Takeuchi T and Choi S 1978 *J. Chem. Phys.* **69** 3672
[33] Parrinello M, Rahman A and Vashishta P 1983 *Phys. Rev. Lett.* **50** 1073
[34] Takeuchi T 1988 *Phys. Stat. Sol. (b)* **147** K9
[35] Stafford A J, Silbert M, Trullas J and Giro A 1990 *J. Phys.: Condens. Matter* **2** 6631
[36] Tasseven Ç, Trullàs J, Alcaraz O, Silbert M and Giró A 1997 *J. Chem. Phys.* **106** 7286
[37] Matsunaga S 2003 *J. Phys. Soc. Jpn.* **72** 1396
[38] Matsunaga S 2009 *J. Phys.: Conf. Ser.* **144** 012011
[39] Jaswal S S and Sharma T P 1973 *J. Phys. Chem. Solids* **34** 509
[40] Geller S 1967 *Science* **157** 310
[41] Looser H, Mali M, Roos J and Brinkmann D 1983 *Solid State Ionics* **9–10** 1237
[42] Ostapenko G 2001 *Solid State Ionics* **138** 199
[43] Ostapenko G I, Cox A and Ostapenko L A 2002 *J. Solid State Electrochem.* **6** 245
[44] Pauling L 1928 *Zeitschrift für Kristallographie - Crystalline Materials* **67** 377